Circular Quadruple-Ridged Flared Horn Achieving Near-Constant Beamwidth Over Multi-Octave Bandwidth: Design and Measurements

Ahmed Akgiray, *Student Member, IEEE,* Sander Weinreb, *Life Fellow, IEEE,*
William A. Imbriale, *Life Fellow, IEEE,* Christopher Beaudoin, *Member, IEEE*

***Abstract*—A circular quadruple-ridged flared horn achieving almost-constant beamwidth over 6:1 bandwidth is presented. This horn is the first demonstration of a wideband feed for radio telescopes which is capable of accommodating different reflector antenna optics, maintains almost constant gain and has excellent match. Measurements of stand-alone horn performance reveal excellent return loss performance as well as stable radiation patterns over 6:1 frequency range. Physical optics calculations predict an average of 69% aperture efficiency and 13 K antenna noise temperature with the horn installed on a radio telescope.**

***Index Terms*—ultrawideband antennas, horn antennas, ridge waveguides, reflector antenna feeds, aperture antennas, reflector antennas, radio astronomy.**

I. Introduction

EFFICIENT reflector antenna feeds with bandwidth much greater than an octave would greatly benefit radio astronomy as well as other applications in communications and defense systems. The very wide bandwidth provides system versatility and also enables applications where the *simultaneous* use of a wide frequency range is required. The need for wide bandwidth feeds has been more pronounced in the past several years because of the availability of transmitter and receiver amplifiers with multi-octave bandwidth.

Some applications for dual-polarized wide bandwidth feeds within radio astronomy are the following:

1) Observations of pulsed (pulsars) and transient radiation which occur in limited time periods but over many octaves of frequency (0.6 to 3 GHz and 2 to 12 GHz are desired bands). The detection sensitivity and timing accuracy can be enhanced by receiving systems matched to this wide spectrum and the pulsar timing observations are of great interest for the detection of gravitational waves [1],

Manuscript received January 21, 2012; revised May 31, 2012; revised September 3, 2012.

This work was supported in part by NSF grant AST-0431486 through Cornell University for the SKA Technical Development Program.

Part of this research was carried out at the Jet Propulsion Laboratory, California Institute of Technology, under a contract with the National Aeronautics and Space Administration.

A. Akgiray and S. Weinreb are with the Department of Electrical Engineering, California Institute of Technology, Pasadena, CA, 91125 USA e-mail: ahmed@caltech.edu, sweinreb@caltech.edu.

W. A. Imbriale is with the Jet Propulsion Laboratory, California Institute of Technology, Pasadena, CA, 91109 USA e-mail: imbriale@jpl.nasa.gov

C. Beaudoin is with the MIT Haystack Observatory, Westford, MA, 01886 USA e-mail: cbeaudoin@haystack.mit.edu.

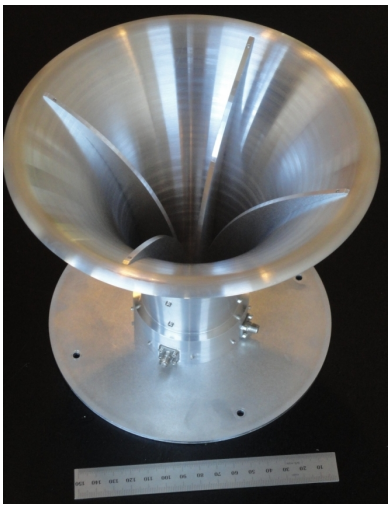

Fig. 1. The circular QRFH covering 2-12 GHz.

2) For very long baseline interferometry (VLBI) observations where large bandwidth (2 to 14 GHz) increases sensitivity and removes fringe ambiguity [2], [3],
3) For measuring the spectral shape (spectral index) of continuum radio sources (such as supernova remnants and quasars) which helps to determine the emission mechanism [4],
4) To search for radio spectral lines with large unknown red-shifts (8 to 50 GHz would be useful),
5) To decrease the cost of large arrays such as the SKA [5], [6] by reducing the number of expensive cryogenic receiver required on thousands of antennas.

While there are multiple dual-polarized wideband feed candidates for next generation radio telescopes, e.g., [7]–[9], the quadruple-ridge flared horn (QRFH) described herein possesses two unique capabilities. Its most distinct feature is the ability to design the horn to have a nearly constant beamwidth over a $\geq$5:1 frequency band for nominal 10 dB beamwidths between 50 and 140 degrees. Therefore, this horn could enable broadband frequency coverage on radio telescopes of different optical configurations. Secondly, the input impedance of this horn could be designed to have a nominal value between 50 and 100 Ohms and requires only one single-ended low-noise amplifier (LNA) per polarization further reducing costs of complex telescope systems.

Ridged waveguides with constant cross-section in the di-

rection of propagation have previously been analyzed using magnetic field integral equations [10], [11] demonstrating possibility of wideband propagation depending on waveguide geometry such as circular, square or diagonal. In contrast, theoretical analysis of ridged horns with cross- sections that flare in the direction of propagation is notably missing from the literature. Therefore, design and development of broadband microwave components employing ridged waveguides with tapered ridges and/or walls have been primarily based on numerical analysis. Many examples of these components are available in the literature, e.g., wideband ortho-mode transducers (OMTs) [12], [13], commercial dual-ridged horns achieving decade bandwidth [14], and quad-ridge horns as reported in [15]–[18].

This article builds upon previous work reported in [19], [20] by discussing electrical design, fabrication and measurements of a circular quadruple-ridge horn covering 2-12 GHz (see Fig. 1). Section II focuses on electrical design and analysis of the QRFH while also briefly discussing mechanical design considerations. Section III presents measured performance of the quad-ridge horn in addition to predicted system performance.

II. Quad-ridge Flared Horn Design and Analysis

The most important physical parameters of the quad-ridge horn used in this work are summarized in Fig. 2. The horn sidewall thickness is not included for clarity; however, the ridge and sidewall taper are shown. The angle β is called the flare angle and is discussed in detail below.

The remainder of this section discusses the required aperture field distributions and aperture mode content to achieve constant beamwidth over 6:1 frequency bandwidth for circular apertures. Various options for ridge and horn profiles to realize the required aperture mode distribution are presented. The section concludes with fabrication considerations.

A. Aperture Mode Content

For aperture antennas such as horns, it is well known that maintaining constant beamwidth as a function of frequency implies that aperture fields must be tapered at the aperture edges with increasing frequency [21]. Furthermore, the aperture field distribution must exhibit circular symmetry if the application requires circular radiation patterns such as the case here. In the case of circular apertures, there has been extensive work in the literature expressing both the aperture field distribution and the resultant radiation patterns in closed form such as those reported in [22], [23].

Using the results of [23], the required aperture field distributions (with uniform phase) to maintain a 10-dB beamwidth of 90 degrees in all azimuthal planes from 2 to 12 GHz are calculated and are shown in Fig. 3 in steps of 1 GHz as a function of normalized aperture radius. This figure clearly shows that achieving such field distributions requires a multitude of modes in the horn.

The aperture mode content required to generate the aperture field distribution is calculated using the technique outlined in [24]. The technique relies on the fact that far-field patterns of all possible modes in a circular aperture horn can be

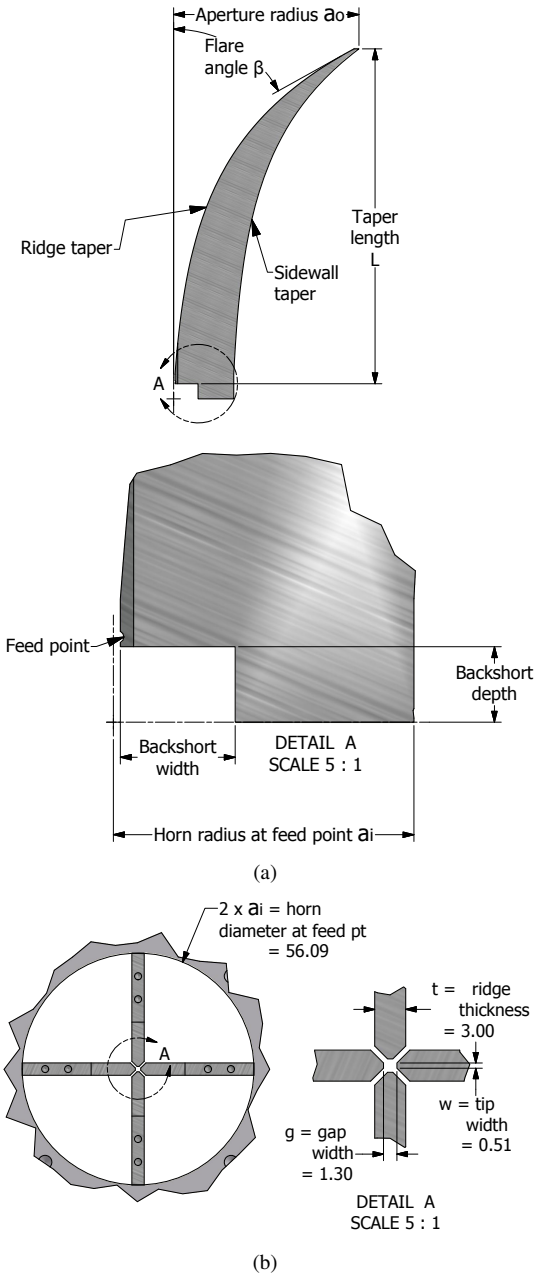

Fig. 2. (a) Ridge side view, (b) view from bottom of feed looking up. The dimensions shown in (b) are as-built dimensions of the QRFH in millimeters. The remaining final dimensions of the QRFH presented herein are: taper length for the ridges and the sidewall are 156.3mm and 151.8mm, respectively; back-short depth and width are 7.04mm and 10.72mm, respectively; the ridge and sidewall aperture radii are, respectively, 83.5mm and 85.8mm; the exponential taper opening rates (see Section II-B) for the ridges and sidewall are 0.0213 and 0.0219, respectively.

expressed by closed-form equations. These are then used as basis functions to express the desired far-field patterns. Te coefficients of this expansion constitute the complex mode amplitudes required at the aperture, the results of this analysis for the aperture field distribution in Fig. 3 are presented in Fig. 4.

These results show that the TE_{11} mode is the dominant mode throughout the frequency range albeit with a decreasing relative power content with increasing frequency. The relative

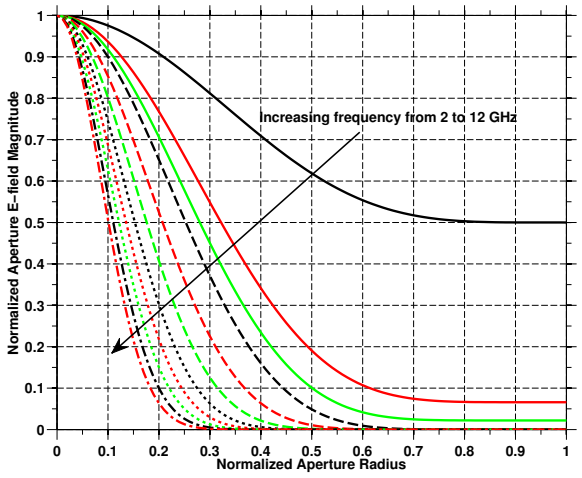

Fig. 3. Normalized aperture field distribution to achieve 10-dB beamwidth of 90 degrees from 2 to 12 GHz using a circular aperture.

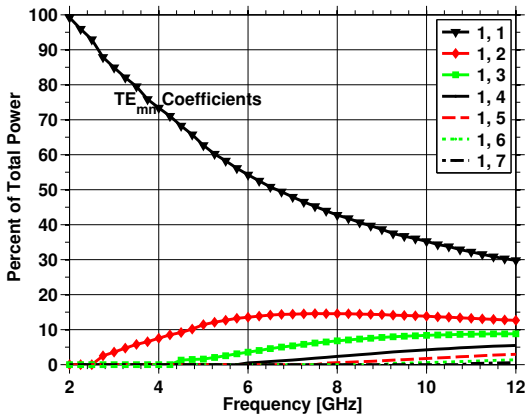

(a)

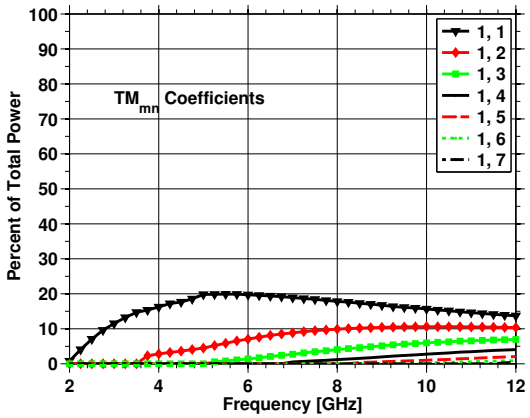

(b)

Fig. 4. (a) TE_{mn}, (b) TM_{mn} mode coefficients to achieve circular radiation patterns with 10-dB beamwidth of 90 degrees from 2 to 12 GHz using a circular aperture of diameter same as the QRFH presented herein.

power in the first four modes, namely $TE_{11}, TE_{12}, TM_{11}$, and TM_{12}, is in good agreement with results presented in [24] for an optimum four-mode horn.

It is also noteworthy to point out that even-order TE or TM modes, i.e., $TE_{0x}, TE_{2x}, \cdots, TM_{0x}, TM_{2x}, \cdots$ are not present. This is because of the perfect two-fold symmetry of the aperture field distribution which prohibits even-order modes.

Having established the necessary mode distribution, the question of how to achieve it remains. The analysis of mode progression along the length of the horn is the topic of ongoing research in our group with the aim of establishing relationship between mode distributions and geometric parameters. Given the lack of such an empirical (or theoretical) relationship, the QRFH development is driven by numerical simulations.

Numerical electromagnetic analysis of antennas spanning multi-octave bandwidths usually requires long simulation times. In order to streamline and accelerate this process, an automated software setup was established early in this research: the quad-ridge horn geometry is represented by approximately 15 parameters; ridge and horn profiles are generated using these parameters in MATLAB [25] and uploaded to the electromagnetic solver CST Microwave Studio (MWS) [26]. Once a simulation is completed, MATLAB retrieves results from CST MWS, performs post-processing to assess "goodness" of data and archives results, and generates a new set of parameters to continue the optimization process. The optimizers used in this work are the simulated annealing and global search routines available in MATLAB which have the advantage of avoiding getting trapped in local minima. The cost function used involves aperture efficiency (calculated using closed-form equations), return loss and also total power as compared to an ideal $\cos^q$ pattern with the desired edge taper. This automated software configuration, running on a dedicated workstation with a graphics processing unit (GPU), has facilitated compilation of an extensive database of quad-ridge horn performance as a function of horn parameters for more than 10000 different geometrical configurations.

B. Exponential Profile

Of all the parameters describing the quad-ridge horn geometry, those that define ridge and sidewall profiles play the most critical role in determining the performance of the horn. Most of the prior work on double- or quadruple-ridged horns focuses on exponential and elliptical profiles for both ridges and sidewall. On the other hand, many more profiles have previously been considered in the literature within the context of corrugated or smooth-wall horn designs [27].

The aforementioned software setup is designed such that the user could choose any of the profiles listed in [27] separately for ridges and sidewall. However, the four most promising functions for quad-ridge horns have been found to be: 1) exponential; 2) elliptical; 3) x^p; and 4) $\tan^p$. The exponential profile is used for both the ridge and sidewall tapers of the QRFH presented herein; thus, we solely focus on that profile in this paper. It is defined as

$$x = A\left(c_1 e^{Rz} + c_2\right) + (1 - A)\left(a_i + (a_o - a_i)\frac{z}{L}\right) \quad (1)$$

where

$$c_1 = \frac{a_o - a_i}{e^{RL} - 1} \quad (2)$$

$$c_2 = \frac{a_i e^{RL} - a_o}{e^{RL} - 1}$$

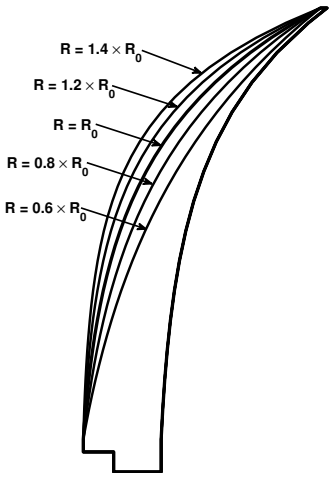

(a)

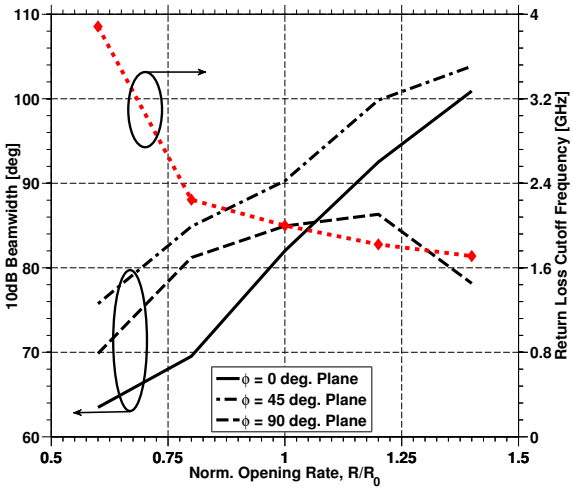

(b)

Fig. 5. (a) Side view of the ridge as exponential opening rate is swept from -40% to +40% of the baseline value R_0, (b) 10 dB beamwidth in $\phi =$ 0, 45, 90 degree planes (at a constant frequency of 5 GHz) and return loss cutoff frequency (cutoff threshold defined as $RL = 10$ dB) as a function of the exponential opening rate of the ridge. $\phi = 0$, 45, 90 curves are plotted using, respectively, solid, dash-dotted and dashed lines. Dotted curve with diamond markers is return loss cutoff frequency.

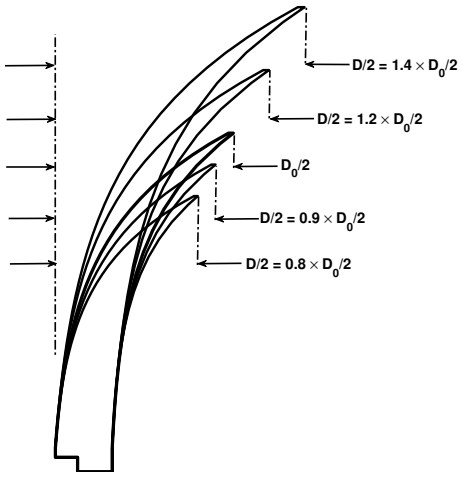

(a)

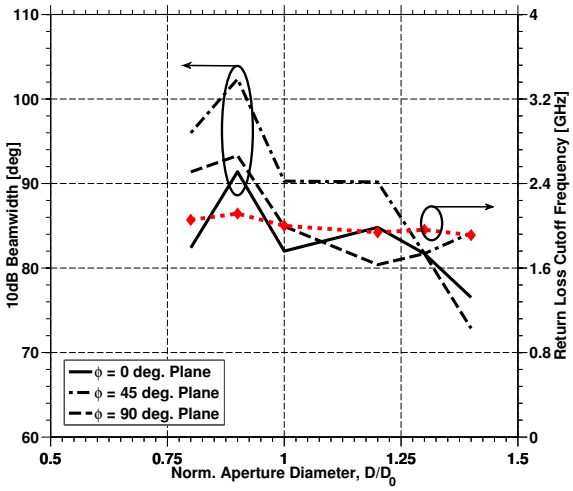

(b)

Fig. 6. (a) Side view of the ridge as aperture diameter is swept from -20% to +40% of the baseline value D_0, (b) 10 dB beamwidth in $\phi =$ 0, 45, 90 degree planes (at a constant frequency of 5 GHz) and return loss cutoff frequency (cutoff threshold defined as $RL = 10$ dB) as a function of aperture diameter. $\phi = 0$, 45, 90 curves are plotted using, respectively, solid, dash-dotted and dashed lines. Dotted curve with diamond markers is return loss cutoff frequency.

and a_i, a_o are, respectively, sidewall radius at the feed point and aperture; R is the exponential opening rate; L is the taper length. The parameter A is between $[0, 1]$ and determines whether a linear taper is added to the profile. The feed point is the point where electromagnetic signal propagating in the horn couples to the coaxial line.

The parameter most influential on the horn's radiation performance is the exponential opening rate of the ridge profile, R. It needs to be selected such that ridge-to-ridge gap is small enough to support propagation of the dominant mode throughout the horn's length while avoiding excessively large or small opening rates which deteriorate return loss.

Another important factor to consider in determining R is due to an interesting property of quad-ridged horns, namely beamwidths in $\phi = 0, 45$ degree planes are determined mainly by the flare angle (β of Fig. 2) rather than aperture size, similar to corrugated horns [28]. H-plane beamwidth of the QRFH, on the other hand, is not as strong a function of the flare angle but depends more on aperture size; thus, it shows more variation with frequency.

To illustrate this point, two sets of simulations are carried out in CST MWS. In the first case, the exponential opening rate is varied $\pm 40\%$ with respect to the as-built value of R_0. Fig. 5(a) shows the simulated ridge profiles with all other parameters fixed. 10 dB beamwidths in $\phi = 0, 45, 90$ degree planes at a constant frequency of 5 GHz are plotted in Fig. 5(b). Strong dependence of beamwidth on flare angle is noted in the $\phi = 0, 45$ degree planes. H-plane beamwidth shows a significantly smaller dependence on the exponential opening rate. Also plotted in the same figure is return loss cutoff frequency, defined as the lowest frequency at which return loss crosses and stays above 10 dB level, which underlines the impact of ridge opening rate on the lowest usable frequency of the horn.

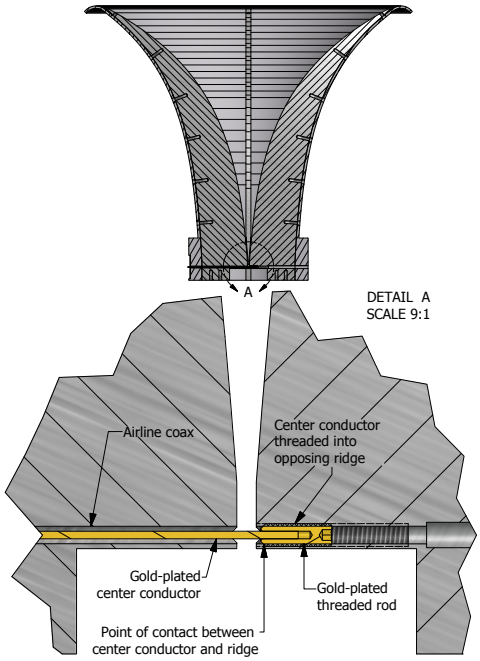

Fig. 7. Detailed view of input coax center conductor connection with opposing ridge. The other two ridges and sidewall are not shown in Detail A for clarity.

For the second set of simulations, aperture diameter of the quad-ridge horn is swept from -20% to $+40\%$ of the as-built value, D_0, while maintaining identical flare angles, which requires scaling of horn's taper length. Resulting profiles are depicted in Fig. 6(a) and Fig. 6(b) plots 10 dB beamwidths and return loss cutoff frequency which show that aperture size has only a secondary effect on beamwidth.

C. Fabrication Considerations

The quad-ridge horn described here has been built in pieces using a numerically controlled milling machine. The base of the horn (i.e. around the feed point) is the most critical part in terms of tolerances on dimensions, locations and orientations of the ridges. Proper location and orientation of ridges are of utmost importance to avoid unwanted higher-order mode excitations due to asymmetry.

A low-loss coaxial air line through one ridge with center conductor connected to the opposite ridge is used to form a balun and excite the ridge waveguide at the base of the horn. The connection of the center conductor of this air line to the opposite ridge is quite critical. An accurate 0.508 mm diameter gold-plated gage pin is welded into a short 0-80 threaded stud which screws into a threaded hole through the opposite ridge. A set screw from the back of the ridge is then utilized to lock the thread of the center conductor. The input end of the center conductor plugs into a well-formed socket of a commercial SMA connector. A small degree of tuning of the feed return loss is accomplished by turning the threaded rod to adjust the contact point in the opposite ridge. These details are provided in the bottom half of Fig. 7.

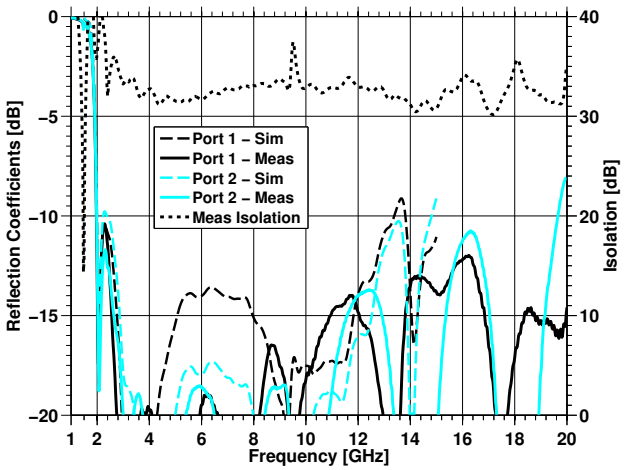

Fig. 8. Measured (solid) and simulated (dashed) reflection coefficients of, and measured isolation (dotted) between both polarizations of the circular QRFH.

III. Measurements

The radiation patterns of the horn were measured using a far-field pattern measurement setup on the roof of the electrical engineering building at California Institute of Technology. Obstacles on the roof limited the accuracy of the patterns to the -25 dB level; but, this is sufficient to determine the main beam, the first side lobes and performance in a reflector system. Both co- and cross-polarized radiation patterns were measured in three azimuthal planes, namely ϕ = 0, 45, and 90 degrees, for θ = [-180, 180] degrees (with one degree steps in the main beam) from 1 to 17 GHz with a frequency resolution of 40 MHz.

A. Scattering parameters and radiation patterns

The circular quad-ridged flared horn covering 2 to 12 GHz is designed to illuminate the secondary reflector of a 12-meter shaped dual-reflector antenna system. The subtended angle at the feed is 100 degrees. In order to balance illumination and spillover efficiencies, the QRFH was designed with target 10-dB beamwidth of 85-90 degrees.

The measured reflection coefficient of both polarizations of the circular quad-ridge horn are shown in Fig. 8 along with the measured isolation between the two polarizations. The measured isolation is better than 30 dB from 2 to 20 GHz while the simulated isolation (not plotted for clarity) is better than 40 dB up to 15 GHz. The return loss is better than 10 dB from 1.95 GHz up to 19 GHz for both ports and significantly better than 15 dB from 2.5 to 11 GHz, implying any mismatch would only have a small effect upon system noise.

The measured and the simulated data sets agree reasonably well with the measured data showing better performance, which is due in large part to the flexibility of the screw-in center conductor. The measured data, shown in Fig. 8, was collected after some minor tuning on both ports which helped improve the return loss beyond 5 GHz. The impact of tuning is more pronounced at higher frequencies (i.e., $\geq$ 10 GHz) where parasitic effects, such as center conductor alignment

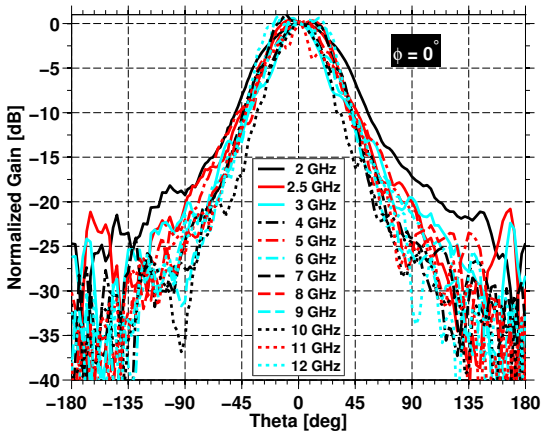

(a)

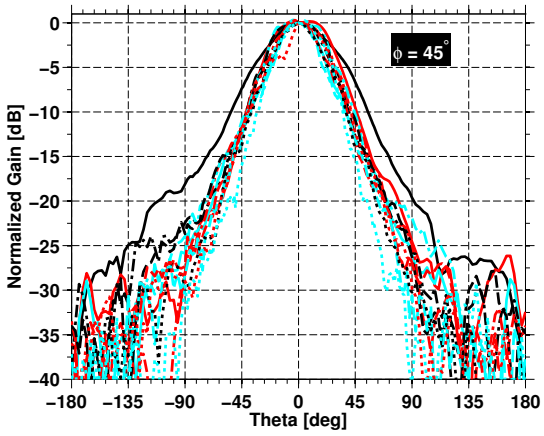

(b)

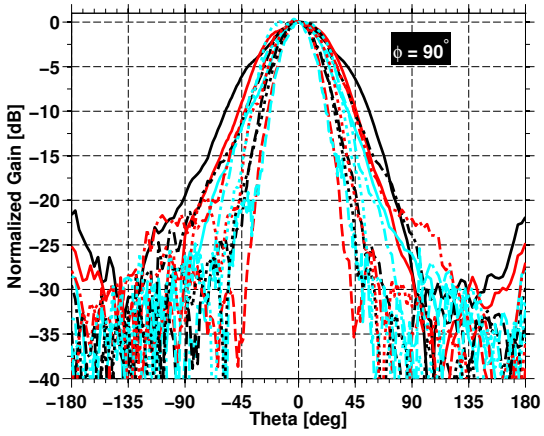

(c)

Fig. 9. Measured far-field patterns of the circular QRFH in (a) $\phi = 0°$, (b) $\phi = 45°$, and (c) $\phi = 90°$ planes from 2 to 12 GHz.

and inductance due to depth of contact with opposite ridge begin to play a bigger role.

The normalized radiation patterns of the QRFH are plotted in Fig. 9 from 2 to 12 GHz in approximately 1 GHz steps in E-, D- and H-planes (see Fig. 11 for unnormalized gain vs frequency). Excellent beamwidth stability is noted in both E- and D-planes. H-plane beamwidth shows more variability—i.e. the far-field patterns are not rotationally symmetric—because of the different boundary conditions on the magnetic

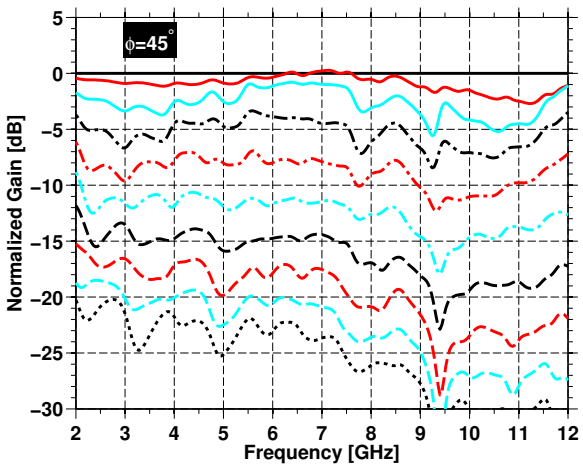

(a)

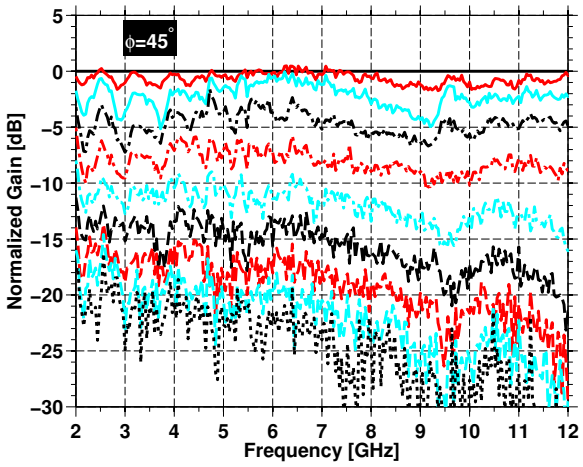

(b)

Fig. 10. (a) Simulated and (b) measured gain vs frequency at θ angles from 0 to 90 degrees in steps of 10 degrees. The curves are at $\phi = 45°$ and are normalized to $\theta = 0°$.

fields in the horn. The radiation patterns of one polarization are plotted for brevity; however, performance of the other polarization is virtually identical. In addition to predicting measured return loss performance quite well, CST MWS does an excellent job estimating the far-zone radiation patterns of the QRFH as shown in Fig. 10. This figure also indicates that high-frequency ripple in measured patterns is an artifact of the far-field range and not due to the horn.

Another parameter of interest to radio astronomy applications is the cross-polarization level of the telescope feed. Fig. 11 presents both measured and simulated peak cross-polarization levels of the QRFH in the $\phi = 45°$ plane with black curves which show that average cross-polarization level of the horn is only about -10 dB. Also shown in the same figure are cross-polarization levels in the secondary patterns computed using physical optics, revealing an average cross-polarization level of -14 dB. The unequal E- and H-plane beamwidth of the QRFH alone only produces secondary cross-polarization of $\leq$ -50 dB.

The cross-polarization performance of the horn is very sensitive to modal content in the horn and could be improved

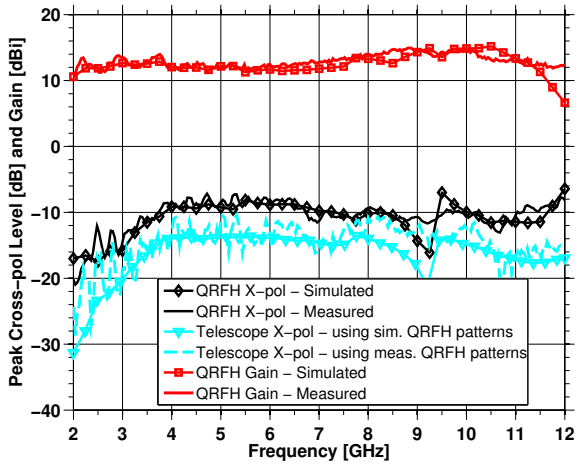

Fig. 11. The measured and simulated gain of the QRFH (top two curves) and peak cross-polarization level of the QRFH (in the $\phi = 45°$ plane) and the GGAO telescope when illuminated by the QRFH.

significantly (e.g. down to -15 dB level) once a thorough understanding of the impact of ridge and sidewall geometry on the mode conversion within the horn is achieved. For radio astronomy applications sensitive to polarization, the cross-polarization can be measured by observations of sources with known polarization and then corrected in data processing. An important criteria is then the stability of the cross polarization which we believe will be very high due to the solid metal construction of the QRFH feed.

The excellent agreement between the CST simulations and measurements shown thus far instills confidence in our modeling of the QRFH as well as the database of QRFH performance as a function of horn parameters generated with the aforementioned automated software setup. This agreement also enables the use of the simulated far-zone patterns in estimating the aperture mode content of the QRFH.

B. Aperture Mode Content

The technique outlined in Section II-A is now used to estimate the mode content at the aperture of the quad-ridge horn. Before proceeding, we note that this is inherently an approximate calculation because the radiation pattern synthesis approach in [24] assumes that the radiating aperture is large compared to the guide wavelength. This is not true in the lower part of the QRFH frequency range. This has two effects: 1) the uniform phase front at the aperture is not planar; 2) the reflections at the aperture, which are ignored, could be important.

Fig. 12 presents the aperture mode analysis results along with aperture efficiency and its sub-efficiencies. Parts (a) and (b) of Fig. 12 plot the fraction of total radiated power in TE_{mn} and TM_{mn} modes, respectively. For this analysis, first 150 TE and 150 TM modes are considered (specifically, those that are above cutoff at the aperture at a given frequency). Only the first six modes are plotted in Fig. 12 for clarity, which is justified because the remaining modes carry little to no power over the operating frequency range. These plots show that TE_{11} is indeed the dominant mode at all frequencies and its behavior

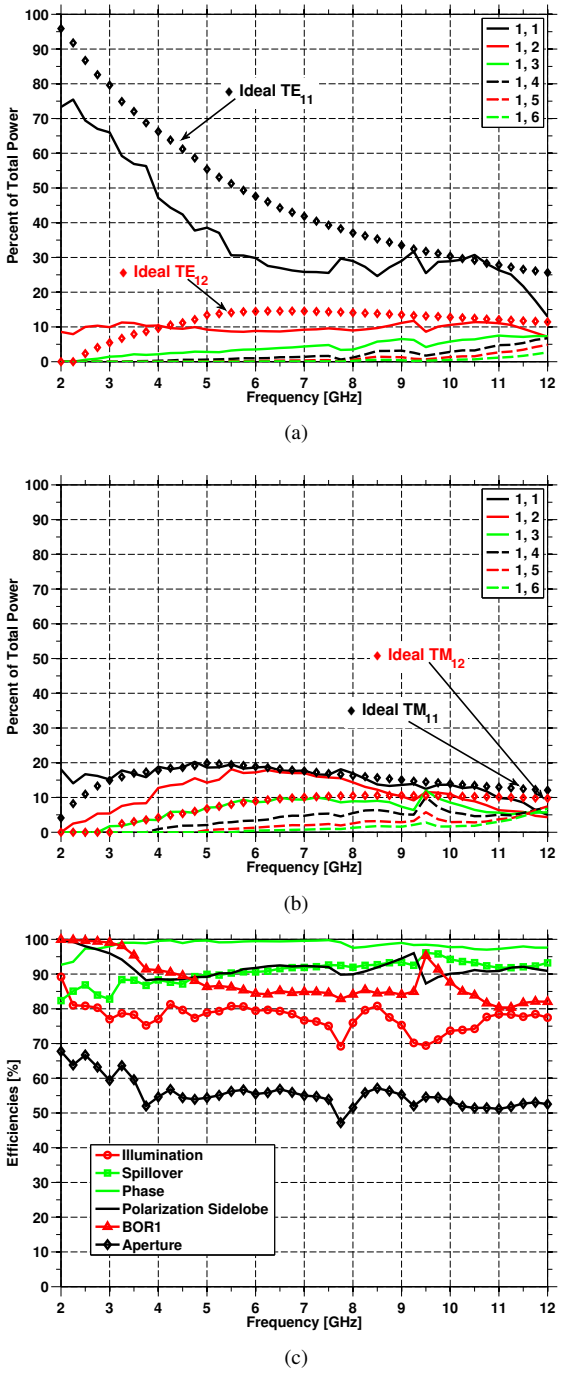

Fig. 12. Percentage of total power in (a) TE_{mn} coefficients and (b) TM_{mn} coefficients; (c) Aperture efficiency and various sub-efficiencies which are calculated using closed-form equations from [29]. Data is based on simulated performance. TE_{11}, TE_{12}, TM_{11}, TM_{12} coefficients from Fig. 4 are reproduced with diamond markers for ease of comparison.

is similar to the required TE_{11} mode amplitude, albeit with a faster decrease in relative power content with increasing frequency. The TE_{12} mode carries roughly the same fraction of the total power regardless of frequency. It is below cutoff at the feed point of the horn all the way up to approximately 8 GHz which implies that it is generated by curvature of ridges and sidewall and is not excited significantly at the feed point.

This, combined with the absence of even-order azimuthal modes, is an important result that suggests that ridges do not significantly alter the mode conversion expected from a smooth-walled horn with the identical profile. In particular, it was shown in [30] that horn diameter variations can only cause coupling between modes of same azimuthal order.

The efficiencies in Fig. 12(c) are calculated using the simulated far-field patterns by closed-form equations from [29], which are intended for prime focus illumination of a reflector; moreover, they do not take into account shaping of the reflector surfaces. Nonetheless, they are presented here for two purposes: 1) they provide a mean to assess contributions of various sub-efficiencies to the overall horn performance; and 2) they capture most of the important features in the far-field radiation patterns.

The illumination efficiency shows a dip around 9.5 GHz which correlates very well with a similar dip observed in Fig. 10. It also corresponds to a small excitation of higher-order TM modes in Fig. 12(b). These modes have the effect of narrowing the main beam in E- and D-planes which manifests itself as reduced illumination efficiency but increased BOR1 efficiency. Due again to this higher-order mode excitation, cross-polarization level in the $\phi = 45$ degree plane increases which can be deduced from polarization sidelobe efficiency curve. A similar dip just below 8 GHz in the aperture efficiency is due mainly to beam narrowing in the H-plane pattern resulting in both reduced illumination and BOR1 efficiencies. The next section presents a more realistic aperture efficiency prediction calculated using physical optics.

C. Predicted System Performance

The shaped dual-reflector radio telescope, for which the QRFH presented herein is designed, was built with optics designed at the Jet Propulsion Laboratory [31] and mechanical design and construction by Patriot/Cobham. The primary reflector has a diameter of 12 meters and the full subtended angle to the secondary reflector is 100 degrees. It is located at the Goddard Geophysical and Astronomical Observatory (GGAO), where it serves as a radio telescope for a geodetic VLBI application requiring 50% aperture efficiency and 50 Kelvin system noise temperature.

A custom physical optics (PO) program, which takes into account shaping of both reflectors, was used to compute both aperture efficiency and antenna noise temperature based upon the measured QRFH patterns. The results for both linear polarizations are shown in Fig. 13.

The predicted aperture efficiency is $\geq$ 65% up to 10 GHz and stays above 50% up to 12 GHz. Aperture efficiency averaged over the entire band is 69%. An important consideration for radio telescopes is phase center stability over the frequency band of interest. The phase center of the QRFH moves approximately 5 cm from 2 to 12 GHz, obtained from measured far-field patterns. Because the PO calculations are carried out for a fixed feed position, the effect of this phase center variation is taken into account. The QRFH is focused at the high end of its frequency band which minimizes loss due to phase center variation as the axial de-focusing at the low end of the band is small compared to a wavelength.

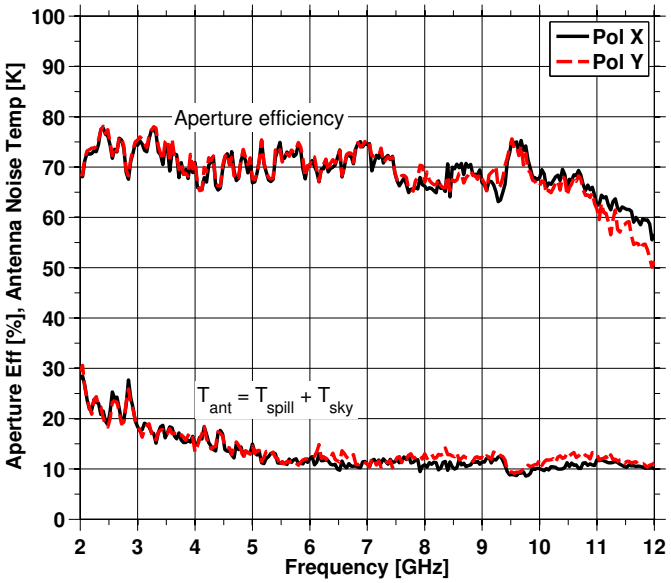

Fig. 13. The predicted aperture efficiency and antenna noise temperature of the circular QRFH designed for the GGAO 12m telescope. Both are calculated using physical optics at an elevation angle of 48 degrees. Losses due to strut and subreflector blockage and r.m.s. surface error are not included in the PO calculations. The sky noise temperature is calculated per the method outlined in [32], and is 5.5K at 4 GHz and 6.5K at 10 GHz.

The predicted antenna noise temperature is less than 20K from 3 to 12 GHz and less than 30 K below 3 GHz. Estimating the receiver noise temperature to be around 23 K (calibration coupler noise contribution 8 K + LNA noise temperature 10 K + coaxial cable loss 5 K), the QRFH-based receiver is expected to meet the 50K T_{sys} and 50% A_{eff} specifications over the entire frequency band. The simulated loss in the horn is less than 0.1 dB corresponding to $<$ 0.8 K noise contribution and is thus negligible. This is because of the solid metal construction and existence of wide surfaces for current flow. Our estimate of the LNA contribution to receiver noise temperature is conservative. Current state-of-the-art cryogenic LNAs developed in our group and in use at GGAO achieve about 6K over much of this band [33]. A new dewar, specifically designed for the QRFH-based receiver, is presently under construction.

IV. Conclusion

A circular quadruple-ridged flared horn is presented that achieves 6:1 frequency bandwidth while maintaining almost constant gain. The measured radiation patterns of the QRFH display very stable beamwidth vs. frequency in E- and D-planes while the H-plane patterns show more variation. The horn exhibits excellent match to 50 Ω from 2 to 19 GHz which is well beyond the target frequency range. Both radiation patterns and scattering parameters are in excellent agreement with simulations. Predicted system performance of the QRFH, based on measured patterns and using physical optics, show an average aperture efficiency $\geq$ 65% and antenna noise temperature less than 30 K over the entire band with an average of 13 K.

The average cross-polarization performance of -10 dB needs improvement but is typical for wideband feeds with greater

than 2:1 frequency ratio currently considered for radio astronomy applications. Modal analysis of the circular QRFH aperture demonstrates that the horn comes fairly close to generating required modes at the aperture to achieve constant beamwidth; however, improvement is necessary to ensure more stable beamwidth vs. frequency, especially in the H-plane.

Further improvements to the cross-pol levels as well as unequal principal plane beamwidths necessitate a better understanding of the mode conversion throughout the horn. Understanding progression of all pertinent modes in the horn with the goal of establishing relationships between ridge/sidewall profiles and mode coupling coefficients and their impact on the quad-ridge horn performance is the topic of ongoing research in our group.

ACKNOWLEDGMENT

The authors would like to thank S. Smith of the California Institute of Technology and D. Hoppe of the Jet Propulsion Laboratory for valuable discussions and suggestions.

REFERENCES

[1] P. Demorest, "A pulsar timing array for gravitational wave detection," presented at the Building on New Worlds, New Horizons: New Science from Sub-millimeter to Meter Wavelengths, Mar. 2011.

[2] A. Niell, A. Whitney, B. Petrachenko, W. Schluter, N. Vandenberg, H. Hase, Y. Koyama, C. Ma, H. Schuh, and G. Tuccari. VLBI2010: Current and future requirements for geodetic VLBI systems. IVS Memorandum 2006-008v01. [Online]. Available: ftp://ivscc.gsfc.nasa.gov/pub/memos/ivs-2006-008v01.pdf

[3] B. Petrachenko. VLBI2010 frequency considerations. IVS Memorandum 2008-015v01. [Online]. Available: ftp://ivscc.gsfc.nasa.gov/pub/memos/ivs-2008-015v01.pdf

[4] J. D. Kraus, *Radio Astronomy*, 2nd ed. Powell, OH: Cygnus-Quasar Books, 1986, ch. 8-3 Source Spectra.

[5] P. J. Hall, Ed., *The SKA: An Engineering Perspective*. The Netherlands: Springer, 2005.

[6] US SKA Consortium, "The square kilometer array preliminary strawman design large N - small D," SKA Memo 18, Jul. 2002.

[7] R. S. Gawande and R. F. Bradley, "Characterization of the active, inverted, conical sinuous antenna," in *XXIX General Assembly of URSI*, Chicago, IL, Aug. 2008.

[8] J. Yang, M. Pantaleev, P.-S. Kildal, Y. Karandikar, L. Helldner, N. Wadefalk, and C. Beaudoin, "Cryogenic 2-13 GHz Eleven feed for reflector antennas in future wideband radio telescopes," *IEEE Trans. Antennas Propag.*, vol. 59, no. 6, pp. 1918–1934, Jun. 2011.

[9] G. Engargiola and W. J. Welch, "Log-periodic antenna," U.S. Patent 6 677 913, Jan. 13, 2004.

[10] W. Sun and C. A. Balanis, "MFIE analysis and design of ridged waveguides," *IEEE Trans. Microw. Theory Tech.*, vol. 41, pp. 1965–1971, Nov. 1993.

[11] ——, "Analysis and design of quadruple-ridged waveguides," *IEEE Trans. Microw. Theory Tech.*, vol. 42, pp. 2201–2207, Dec. 1994.

[12] G. M. Coutts, "Octave bandwidth orthomode transducers for the expanded very large array," *IEEE Trans. Antennas Propag.*, vol. 59, no. 6, pp. 1910–1917, Jun. 2011.

[13] C. Granet and G. L. James, "The quad-ridged omt: The effects of fin shape on performance," CSIRO, Australia, Tech. Rep. RPP 3879, Oct. 1996.

[14] V. Rodriguez, "Recent improvements to dual ridge waveguide horn antennas: The 200MHz to 2000MHz and 18GHz to 40GHz models," in *2009 IEEE International Symposium on Electromagnetic Compatibility*, Austin, TX, Aug. 2009.

[15] O. B. Jacobs, J. W. Odendaal, and J. Joubert, "Elliptically shaped quad-ridge horn antennas as feed for a reflector," *IEEE Antennas Wireless Propag. Lett.*, vol. 10, pp. 756–759, Jul. 2011.

[16] S. A. Soroka, "A physically compact quad ridge horn design," in *1986 Antennas and Propagation Society International Symposium*, Jun. 1986.

[17] R. J. Bauerle, R. Schrimpf, E. Gyorko, and J. Henderson, "The use of a dielectric lens to improve the efficiency of a dual-polarized quad-ridge horn from 5 to 15 GHz," *IEEE Trans. Antennas Propag.*, vol. 57, no. 6, pp. 1822–1825, Jun. 2009.

[18] M. Gilbert, K. Higgins, and L. Romero, "Quad-ridge horn utilizing resistive films to reduce sidelobes," in *2007 IEEE Antennas and Propagation Society International Symposium*, Jun. 2007.

[19] A. Akgiray, S. Weinreb, and W. A. Imbriale, "Wideband near-constant beamwidth flared quad-ridge horn feed for reflector antennas in radio astronomy," presented at the USNC-URSI National Radio Science Meeting, Boulder, CO, Jan. 2011.

[20] ——, "Design and measurements of dual-polarized wideband constant-beamwidth quadruple-ridged flared horn," in *Proc. 2011 IEEE International Symposium on Antennas and Propagation (APSURSI)*, Spokane, WA, Jul. 2011.

[21] C. A. Balanis, *Antenna Theory: Analysis and Design*, 3rd ed. New Jersey: Wiley, 2005.

[22] R. C. Hansen, "A one-parameter circular aperture distribution with narrow beamwidth and low sidelobes," *IEEE Trans. Antennas Propag.*, vol. AP-25, pp. 477–480, Jul. 1976.

[23] D.-W. Duan and Y. Rahmat-Samii, "A generalized three-parameter aperture distribution for antenna applications," *IEEE Trans. Antennas Propag.*, vol. 40, no. 6, pp. 697–713, Jun. 1992.

[24] A. C. Ludwig, "Radiation pattern synthesis for circular aperture horn antennas," *IEEE Trans. Antennas Propag.*, vol. AP-14, no. 4, pp. 434–440, Jul. 1966.

[25] MATLAB version 7.10.0. Natick, MA: The Mathworks, Inc., 2010.

[26] CST Microwave Studio 2011. Darmstadt, Germany: CST AG, 2011.

[27] C. Granet, "Profile options for feed horn design," in *2000 Asia-Pacific Microwave Conference*, Sydney, NSW, Australia, Dec. 2000.

[28] M. Abbas-Azimi, F. Mazlumi, and F. Behnia, "Design of broadband constant-beamwidth conical corrugated-horn antennas [antenna designer's notebook]," *IEEE Antennas Propag. Mag.*, vol. 51, pp. 109–114, Oct. 2009.

[29] P.-S. Kildal, *Foundations of Antennas A Unified Approach*. Lund, Sweden: Studentlitteratur, 2000.

[30] J. L. Doane, *Infrared and Millimeter Waves*. Orlando, FL, USA: Academic Press, 1985, vol. 13 Millimeter-wave Components and Techniques Part IV, ch. 5.

[31] W. A. Imbriale, "Radio frequency optics design of the 12-meter antenna for the array-based deep space network," Jet Propulsion Laboratory/NASA, Pasadena, CA, USA, IPN Progress Report 42-160, Feb. 2005.

[32] G. C. Medellin, "Antenna noise temperature calculation," SKA Memo 95, Jul. 2007.

[33] J. D. Pandian, L. Baker, G. Cortes, P. F. Goldsmith, A. A. Deshpande, R. Ganesan, J. Hagen, L. Locke, N. Wadefalk, and S. Weinreb, "Low-noise 6-8 GHz receiver," *IEEE Microwave Magazine*, vol. 7, no. 6, Dec. 2006.

Ahmed H. Akgiray has been a student member of the IEEE since 2003. He received the B.S. degree in Electrical Engineering at Cornell University in 2005, and M.S. degree in Electrical Engineering at University of Illinois at Urbana-Champaign, in 2007, with a thesis entitled "Calibration of Jicamarca Radar Using F-region Incoherent Scatter For Measurements of D-region Backscatter RCS."

He, then, joined the Jet Propulsion Laboratory where he worked from May 2007 to May 2010. His responsibilities included lead RF/Microwave test engineer role for an assembly of landing radar of the Mars Science Laboratory (landed on Mars in August 2012) during which he oversaw assembly, testing and troubleshooting of 30+ engineering and spaceflight modules from the first test to final qualification. At JPl, he also performed most of the RF design work of the frequency synthesizer assembly of the Soil Moisture Active and Passive (SMAP) satellite radar. While still at Cornell, he worked at the MIT Haystack Observatory during the summer of 2004 on radio frequency cryogenic LNA design. He is currently pursuing a PhD degree at the California Institute of Technology focusing on wideband antenna and LNA development.

Mr. Akgiray was awarded for outstanding academic record at Cornell University, was listed on the Outstanding Teaching Assistants List at the University of Illinois, and received two awards while at the Jet Propulsion Laboratory. He is the author of a 2011 IEEE Antennas and Propagation Symposium Student Paper Competition Honorable Mention paper as well as a co-author on two journal articles with Prize Paper awards.

Sander Weinreb Sander Weinreb is presently a Principal Scientist at JPL and a Faculty Associate at Caltech. He received the B.S.E.E. and Ph.D. degrees from M.I.T. in 1958 and 1963 respectively. Most of his career has been in the administration or development of instrumentation in radio astronomy. From 1966 to 1988 he led the Electronic Division of National Radio Astronomy Observatory where he was responsible for the design of all electronics for the Very Large Array and all other telescopes operated by the observatory. In 1989 he joined the central research laboratory of Martin Marietta where he led the millimeter-wave integrated circuit design and test group until 1996. He has had interim teaching positions at UC Berkeley, U. of Virginia, and U. of Massachusetts before joining JPL and Caltech in 1999.

Dr. Weinreb's major accomplishments are the introduction of digital correlation techniques into radio astronomy, the discovery of the first cosmic molecular spectral line (OH) and the introduction of cryogenic transistor amplifiers to radio astronomy. He has over 150 publications, has served on many review and visiting committees, is a Life Fellow of the IEEE, and was the recipient of the both the 2008 Reber Medal and the 2010 Jansky Award for innovative lifetime contributions to radio astronomy. His current research activities are in the areas of cryogenic low noise amplifiers and decade bandwidth antenna feeds.

William A. Imbriale received a B.S. degree in engineering physics from Rutgers University in 1964; an M.S. degree in electrical engineering from the University of California, Los Angeles, in 1966; and a Ph.D. degree from the University of Illinois in 1969.

Dr. Imbriale is a senior research scientist in the Communications Ground System Section at the Jet Propulsion Laboratory, California Institute of Technology. Since starting at JPL in 1980, he has led many advanced technology developments for large ground-station antennas, lightweight spacecraft antennas, and millimeter-wave spacecraft instruments. He has recently returned from a 6 month sabbatical at University of California, San Diego where he taught an advanced Antenna Engineering class and did research on microwave devices and mm-wave Radio Telescopes. Prior to that, he was involved in the design of the Square Kilometre Array. Previously he completed a technology contract for the Earth Sciences Technology Office to develop a subreflector consisting of MEMS switches integrated with patch reflect array elements that will compensate, in real time, for on-orbit distortions of a membrane inflatable antenna. He was also the lead engineer for the Spanish supplied High Gain Antenna System for the Mars Science Laboratory rover. He has also worked on the Deep Space Network (DSN) Large Array, a concept to significantly increase the capability of the DSN by arraying a large number of inexpensive small antennas. He has developed technologies to enable the use of Ka-band frequencies on NASAs DSN 70-meter antennas, by overcoming the substantial gain loss due to gravity-induced distortions as a function of elevation angle.

During the 1980s, Dr. Imbriale managed the Radio Frequency and Microwave Subsystem Section, which was responsible for the research, development, and implementation of RF and microwave subsystems used in the DSN. From 1969 to 1980, Dr. Imbriale was employed at the TRW Defense and Space Systems Group where he was the Subproject Manager for the Antennas of the NASA Tracking and Data Relay Satellite System program.

He has published two books in the JPL Monograph series on Deep Space Communications (Imbriale, Large Antennas of the Deep Space Network, John Wiley and Sons, 2003) and (Imbriale, Spaceborne Antennas for Planetary Exploration, John Wiley and Sons, 2006). His most recent book, Space Antenna Handbook, was published in 2012.

Dr. Imbriale is a Life Fellow of the IEEE; a member of the URSI Commission B; and a member of the Sigma Xi, Tau Beta Pi, and Eta Kappa Nu honor societies. He has received numerous NASA honor awards, including the Exceptional Service Medal. He also received the Rutgers Distinguished Engineering award in 2012. From 1993 through 1995, he was a distinguished lecturer for the Antennas and Propagation Society, speaking on beam-waveguide antennas and the evolution of the DSN antennas. He has published extensively and has won three best paper awards. He was a member of the Administration Committee of the IEEE Antennas and Propagation Society and general chairman of the 1995 International IEEE Antennas and Propagation International Symposium, held in Newport Beach, California. He has lectured and taught engineering courses at several learning institutions, including the University of California, Los Angeles, the University of California, San Diego and the University of Southern California. He is also a consultant to industry on all aspects of antenna analysis and design.

Christopher J. Beaudoin was born in Peterboro, NH, on October 21, 1977. He received the D.ENG degree in electrical engineering from the University of Massachusetts Lowell (UML) in 2006 for research in physical scale modeling of UHF radar signatures. At the UML Submillimeter Wave Technology Laboratory, he was employed as a senior electrical engineer and conducted research in airborne/ground-based synthetic aperture radar (SAR), designed/constructed compact radar range instrumentation, and developed SAR signal processing algorithms for scale model acquisition of full scale radar signatures. As a natural extension of his radar studies, he also conducted research in computational electromagnetic scattering and analyses in support of the laboratories' signature solution responsibilities.

In 2008, Dr. Beaudoin joined the research staff at the MIT Haystack Observatory as a research engineer. In this role, he is a member of the team developing NASA's next generation microwave system for the geodetic Very Long Baseline Interferometry (VLBI) program, an effort that will reduce the uncertainty in network telescope positions to 1 millimeter on global scales. His contributions to this effort include the design of an ultra low noise (50 Kelvin)/broadband (2-14 GHz) cryogenic front-end, electromagnetic analysis for radio telescope RFI mitigation, development of signal processing algorithms for geodetic delay extraction, and the innovation of monitor/control infrastructure for the NASA geodetic VLBI radio telescope network.